

The $^{39}\text{K}_2$ $2^3\Sigma_g^+$ state: Observation and analysis

Dan Li, Feng Xie, and Li Li^{a)}

Department of Physics, Tsinghua University, Beijing 100084, China and Key Laboratory of Atomic and Molecular Nanosciences, Tsinghua University, Beijing 100084, China

Vladimir B. Sovkov and Valery S. Ivanov

V. A. Fock Institute of Physics, St. Petersburg State University, 1 Ulyanovskaya Street, Petrodvorets, St. Petersburg 198504, Russia

Ergin Ahmed and A. Marjatta Lyyra

Department of Physics, Temple University, Philadelphia, Pennsylvania 19122

John Huennekens

Department of Physics, Lehigh University, Bethlehem, Pennsylvania 18015

Sylvie Magnier

Laboratoire de Physique des Atomes, Lasers, Molécules et Surfaces (PALMS), CNRS et Université Rennes 1 (UMR 6627), Campus de Beaulieu, Bt 11B 35042 Cedex, France

(Received 8 January 2007; accepted 22 March 2007; published online 21 May 2007)

The $^{39}\text{K}_2$ $2^3\Sigma_g^+$ state has been observed by perturbation-facilitated infrared-infrared double resonance spectroscopy and two-photon excitation. Resolved fluorescence spectra into the $a^3\Sigma_u^+$ state have been recorded. The observed vibrational levels have been assigned as the $v=23-25$, 27, 28, 31-33, 38-45, 47, and 53 levels by comparing the observed and calculated spectra of the $2^3\Sigma_g^+ \rightarrow a^3\Sigma_u^+$ transitions. Molecular constants have been obtained using a global fitting procedure with a comprehensive set of experimental data. Fine and hyperfine splittings have been resolved in the excitation spectra. Perturbations between the $2^3\Sigma_g^+$ and $2^3\Pi_g$ states were observed. The hyperfine patterns of the $2^3\Sigma_g^+$ levels are strongly affected by the perturbation. The perturbation-free and weakly perturbed levels follow the case $b_{\beta S}$ coupling scheme, while the perturbed levels follow case $b_{\beta J}$ coupling. A Fermi contact constant, $b_F=65\pm 10$ MHz, has been obtained. Intensity anomalies of rotational lines appeared both in the $2^3\Sigma_g^+ \sim 2^3\Pi_g \leftarrow b^3\Pi_u$ excitation spectra and in the $2^3\Sigma_g^+ \sim 2^3\Pi_g \rightarrow a^3\Sigma_u^+$ resolved fluorescence spectra. These intensity anomalies can be explained in terms of a quantum-mechanical interference effect. © 2007 American Institute of Physics. [DOI: 10.1063/1.2730804]

I. INTRODUCTION

Triplet state spectra provide a wealth of information concerning hyperfine structure and spin-orbit, spin-spin, and spin-rotation interactions that is not available from singlet state spectra. However, the ground state of all alkali dimers is a singlet state, $X^1\Sigma_g^+$, and experimental observation of triplet states is much more difficult than the observation of singlet states. Perturbation-facilitated optical-optical double resonance (PFOODR) spectroscopy uses a two-step excitation scheme through singlet \sim triplet mixed intermediate levels: a *pump* laser excites from the singlet ground state, $X^1\Sigma_g^+$, to an $A^1\Sigma_u^+ \sim b^3\Pi_u$ mixed level, then a *probe* laser further excites into high-lying triplet states. Resolved fluorescence from high-lying triplet states provides information on both the high-lying states and the low-lying $a^3\Sigma_u^+$ and $b^3\Pi_u$ states.¹⁻³ This PFOODR spectroscopic technique has been used to study triplet states of the Li_2 , Na_2 , K_2 , and NaK molecules.^{3,4} Recently, the $2^3\Pi_g$ state of K_2 has been studied by perturbation-facilitated infrared-infrared (IR-IR) double

resonance with two tunable diode lasers.⁵⁻⁷ The present work reports our study of the K_2 $2^3\Sigma_g^+$ state.

II. EXPERIMENT

The IR-IR double resonance and two-photon excitation experimental setups have been described in Refs. 5 and 7. Briefly, potassium vapor was generated in a heat pipe oven, and 1 Torr of Ar was used as a buffer gas. In the IR-IR double resonance experiment, two single mode tunable diode lasers were used as the pump and probe lasers. The pump laser selectively excited an $A^1\Sigma_u^+ \sim b^3\Pi_u$ mixed intermediate rotational level from the singlet ground state; the probe laser frequency was scanned and transitions into the $2^3\Sigma_g^+$ state were monitored by detecting visible $2^3\Sigma_g^+ \rightarrow a^3\Sigma_u^+$ fluorescence. When the pump and probe lasers excited an upper $2^3\Sigma_g^+$ level, the $2^3\Sigma_g^+ \rightarrow a^3\Sigma_u^+$ fluorescence was collected and dispersed by a Spex 1404 monochromator. In the two-photon excitation case, one laser (either a diode laser or a CR 899-29 Ti:sapphire laser) was used.

For purposes of assigning the two-photon fluorescence spectrum, a second heat pipe oven containing a sodium-potassium mixture was also used in a similar setup. In this

^{a)}Author to whom all correspondences should be addressed.

case, the oven temperature was $\sim 380^\circ\text{C}$, and the argon pressure ~ 1.25 Torr. We estimated the ratio of $\text{K}_2/\text{NaK}/\text{Na}_2$ vapor pressures to be 5.1/2.8/1.0 in this oven. A few hundred milliwatts of Ti:sapphire laser power was used and resolved fluorescence was recorded with a 0.3 m McPherson monochromator and photomultiplier tube combination used in a photon counting mode.

III. RESULTS

A. The $2^3\Sigma_g^+ \rightarrow a^3\Sigma_u^+$ fluorescence: electronic and vibrational assignments

Theoretical potentials have been calculated for 98 electronic states of K_2 below the $\text{K}(4s)+\text{K}(5d)$ atomic limit.⁸ In our probe region (21 100–24 000 cm^{-1} above the potential minimum of the ground state), five electronic states could have been excited from the $A^1\Sigma_u^+ \sim b^3\Pi_u$ mixed intermediate levels: the $2^3\Pi_g$, $1^3\Delta_g$, $2^3\Sigma_g^+$, $3^1\Sigma_g^+$, and $4^1\Sigma_g^+$ states. Among these five states, only the $2^3\Pi_g$ and $2^3\Sigma_g^+$ can radiate to the $a^3\Sigma_u^+$ state. Previously, the $2^3\Pi_g v=0-42$ levels of K_2 have been observed and the $2^3\Pi_g \rightarrow a^3\Sigma_u^+$ fluorescence has been resolved.⁵⁻⁷ The $\text{K}_2 2^3\Pi_g \rightarrow a^3\Sigma_u^+$ fluorescence has a very similar pattern to the $2^3\Pi_g \rightarrow a^3\Sigma_u^+$ fluorescence of Li_2 and Na_2 .⁹⁻¹¹ The Mulliken difference potentials^{12,13} of the $2^3\Pi_g$ and $a^3\Sigma_u^+$ states of Li_2 , Na_2 , and K_2 are not monotonic; hence, quantum interference structure appears in the fluorescence spectra from higher vibrational levels. The $2^3\Sigma_g^+ \rightarrow a^3\Sigma_u^+$ fluorescence pattern of K_2 , however, is quite different from the pattern of the $2^3\Pi_g \rightarrow a^3\Sigma_u^+$ fluorescence. Figure 1 shows the resolved fluorescence from the $2^3\Sigma_g^+ v=23, N=43$ level. Spectrum A was recorded when the pump laser ($11\,548.035\text{ cm}^{-1}$) and probe laser (9633.499 cm^{-1}) excited the $2^3\Sigma_g^+ v=23, N=43 \leftarrow b^3\Pi_{0u} v'=19, J'=42 \leftarrow X^1\Sigma_g^+ v''=0, J''=43$ transition; spectrum B corresponds to excitation with the pump laser only; and spectrum C is spectrum A–spectrum B, corresponding to the *net* fluorescence from the upper $2^3\Sigma_g^+ v=23, N=43$ level to the $a^3\Sigma_u^+$ state. The Mulliken difference potential curve of the $\text{K}_2 2^3\Sigma_g^+$ and $a^3\Sigma_u^+$ states calculated from *ab initio* potential curves⁸ shows no extrema, and the vibrational quantum number of the upper state can be determined simply by node counting. In the case of Fig. 1, the vibrational quantum number of the upper level is 23.

In Fig. 1, spectrum B was recorded with the pump laser alone. In this spectrum, we observe a diffuse band which has a maximum at 574 nm. This kind of diffuse band has been observed under various excitation conditions in Li_2 (peaking at 458.5 nm),¹⁴ Na_2 (peaking at 436.5 nm)¹¹ and K_2 (peaking at ~ 574 nm),¹⁵ and in each case the origin was found to be $2^3\Pi_g \rightarrow a^3\Sigma_u^+$ transitions.¹¹ The $2^3\Pi_g \rightarrow a^3\Sigma_u^+$ 436 nm diffuse band of Na_2 has been observed whenever an $A^1\Sigma_u^+$ (or $b^3\Pi_u$) $\leftarrow X^1\Sigma_g^+$ transition was excited.¹⁶ The $2^3\Pi_g$ state was populated by collisions of two excited Na_2 molecules in the $A^1\Sigma_u^+$ (or $b^3\Pi_u$) state (energy pooling). The 574 nm diffuse band of K_2 seen in spectrum B could be produced by the same collision mechanism as in Na_2 . The residual of this 574 nm peak in spectrum C might be due to collisions of the $b^3\Pi_u$ molecules populated by $2^3\Sigma_g^+ \rightarrow b^3\Pi_u$ radiation. The $2^3\Sigma_g^+ v=23$ level is $\sim 300\text{ cm}^{-1}$ below the $2^3\Pi_g v=0$ level

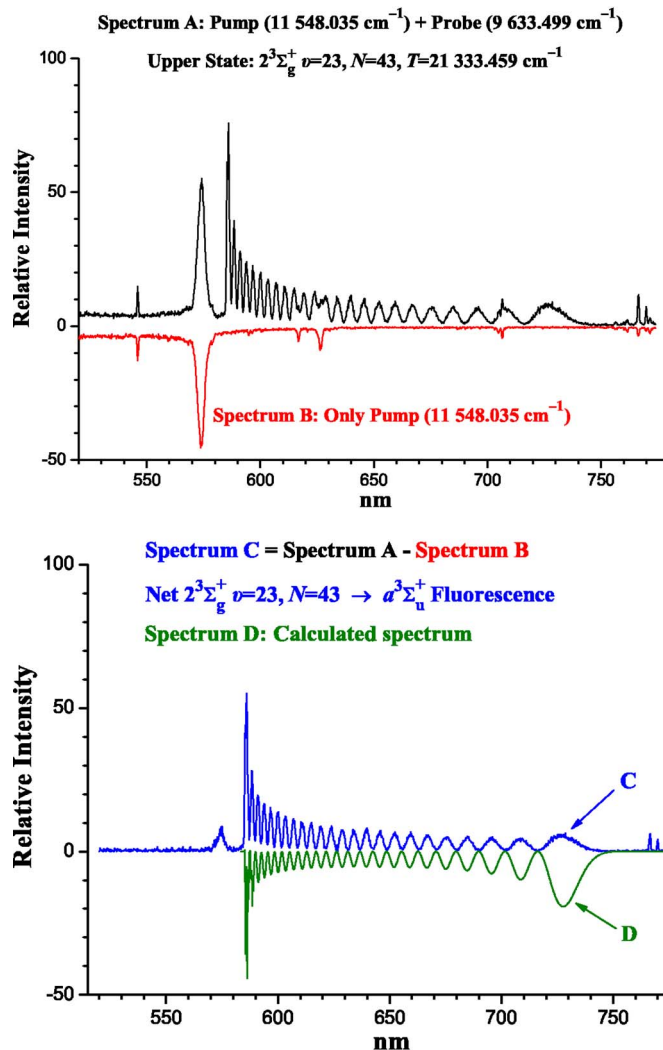


FIG. 1. Resolved fluorescence of the $2^3\Sigma_g^+ v=23, N=43 \rightarrow a^3\Sigma_u^+$ transition. Spectrum A was recorded when the pump laser ($11\,548.035\text{ cm}^{-1}$) and probe laser (9633.499 cm^{-1}) excited the $2^3\Sigma_g^+ v=23, N=43 \leftarrow b^3\Pi_{0u} v'=19, J'=42 \leftarrow X^1\Sigma_g^+ v''=0, J''=43$ transition; spectrum B was recorded with only the pump laser present; and spectrum C is the difference between the two (spectrum A–spectrum B). The features at 546.0, 616.8, 626.5, and 706.5 nm in spectra A and B are due to scattered room lights. Spectrum C is the net fluorescence from the upper $2^3\Sigma_g^+ v=23, N=43$ level to the $a^3\Sigma_u^+$ state. Spectrum D is the simulation. The experimental intensities have not been corrected for the relative detection system efficiency vs wavelength.

and the contribution from $2^3\Sigma_g^+ \rightarrow 2^3\Pi_g$ collisions to this 574 nm peak is therefore expected to be small.

B. Perturbation and quantum interference

We have also observed perturbations between the $\text{K}_2 2^3\Sigma_g^+$ and $2^3\Pi_g$ states. Figure 2 shows the resolved fluorescence spectra from the mutually perturbed $2^3\Pi_{0g} v=16, J=71$ and $2^3\Sigma_g^+ v=40, N=71, J=71$ levels to the $a^3\Sigma_u^+$ state. As seen in Fig. 2(a), in the 545–585 nm region, both spectra look similar to the spectrum from the unperturbed (or only weakly perturbed) $2^3\Pi_g v=15$ levels [Fig. 3(a)]. However, from the mixed levels, an additional oscillating continuum at wavelengths longer than 580 nm appears in both spectra [Fig. 2(b)]. While the 574 nm peak and emission at shorter wavelengths [see Fig. 2(a)] is stronger in the $2^3\Pi_g \rightarrow a^3\Sigma_u^+$ spectrum (lower) than in the $2^3\Sigma_g^+ \rightarrow a^3\Sigma_u^+$ spectrum (up-

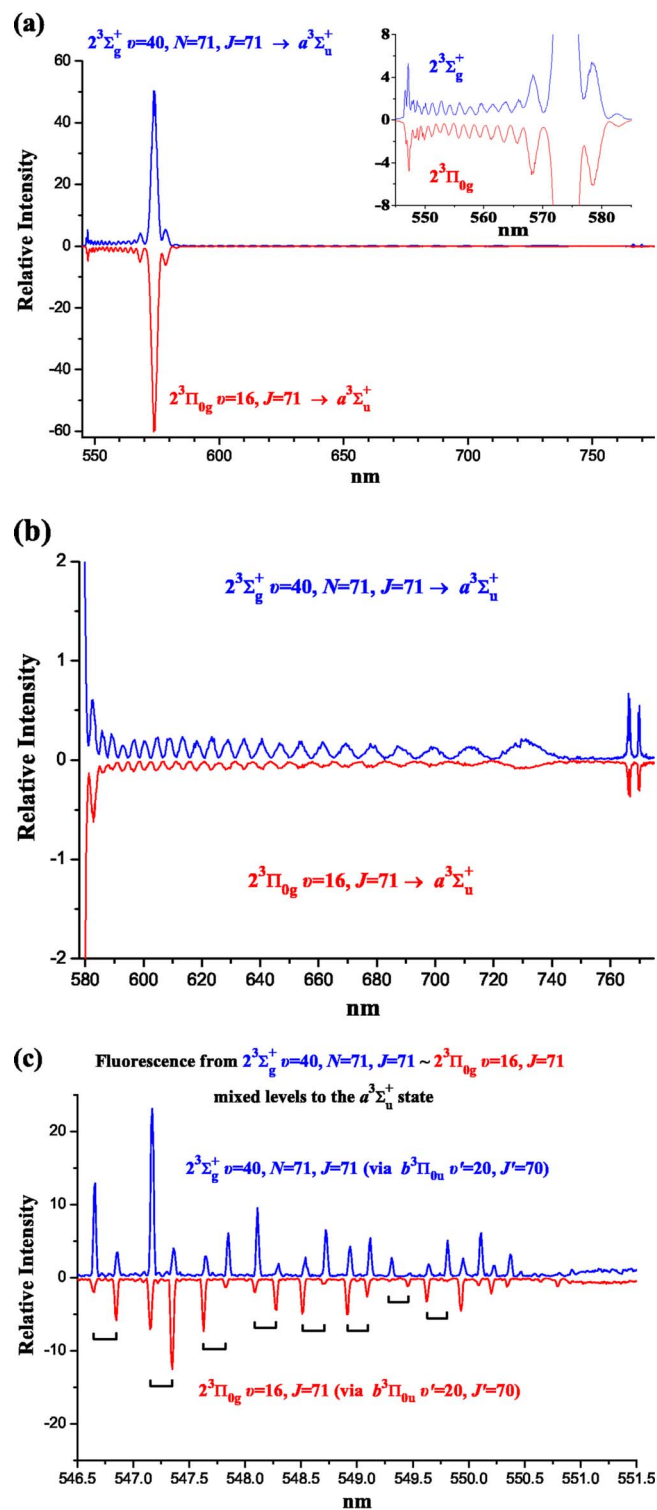


FIG. 2. Resolved fluorescence spectra from the mutually perturbed $2^3\Pi_{0g} v=16, J=71$ and $2^3\Sigma_g^+ v=40, N=71, J=71$ levels to the $a^3\Sigma_u^+$ state. (a) Full spectra showing bound-bound and bound-free parts; inset shows close-up of the 545–585 nm region. (b) Enlargement of the bound-free emission in the spectral range of 578–775 nm. (c) Bound-bound part of the spectra (546.5–551.5 nm) with higher resolution. Some R, P line pairs have been marked by brackets.

per), the intensity of the $\lambda > 580$ nm oscillating continuum [Fig. 2(b)] in the $2^3\Sigma_g^+ \rightarrow a^3\Sigma_u^+$ spectrum (upper) is stronger than that in the $2^3\Pi_{0g} \rightarrow a^3\Sigma_u^+$ spectrum (lower), indicating that the origin of the 574 nm peak and associated continuum is the $2^3\Pi_g$ state and the fluorescence at $\lambda > 580$ nm is due

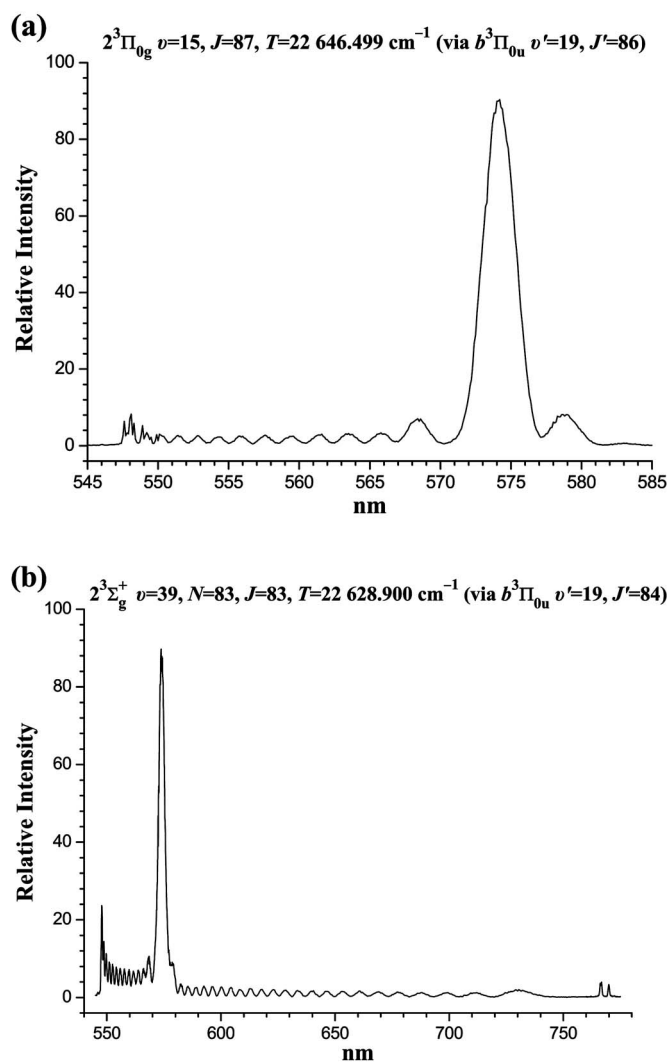


FIG. 3. (a) Fluorescence spectrum from the very weakly perturbed $2^3\Pi_{0g} v=15, J=87$ level. (b) Fluorescence spectrum from the $2^3\Sigma_g^+ v=39, N=83, J=83$ level.

to the $2^3\Sigma_g^+$ state. An analogous picture can be observed for other perturbed levels as well. For example, Fig. 3(b) shows the resolved fluorescence spectrum from another perturbed $2^3\Sigma_g^+$ level ($v=39, N=83, J=83$).

Figure 2(c) is an expanded portion of Fig. 2(a) showing transitions into the bound levels of the $a^3\Sigma_u^+$ state. Unlike the rotational pattern from unperturbed $2^3\Pi_g$ and $2^3\Sigma_g^+$ levels, where the P - R lines have nearly the same intensities, in Fig. 2(c), the P - R lines have quite different intensities into each $a^3\Sigma_u^+ v'$ level.

It is well known that when probabilities of transitions from two interacting states to a common level are comparable in value, rotational line intensity anomalies can occur due to quantum-mechanical interference effects.¹⁷ This type of rotational line intensity anomaly has been observed both in the $2^3\Pi_{0g} \sim 2^3\Sigma_g^+ \leftarrow b^3\Pi_{0u}$ excitation spectra and in the $2^3\Pi_{0g} \sim 2^3\Sigma_g^+ \rightarrow a^3\Sigma_u^+$ resolved fluorescence spectra of K_2 . The $2^3\Pi_{0g} v=16, J=71$ and $2^3\Sigma_g^+ v=40, N=71, J=71$ levels are mutually perturbed levels and both levels have non-zero transition probabilities from the $b^3\Pi_{0u} v'=20, J'=70$ intermediate level. While the intensities of the $2^3\Pi_{0g} v=16,$

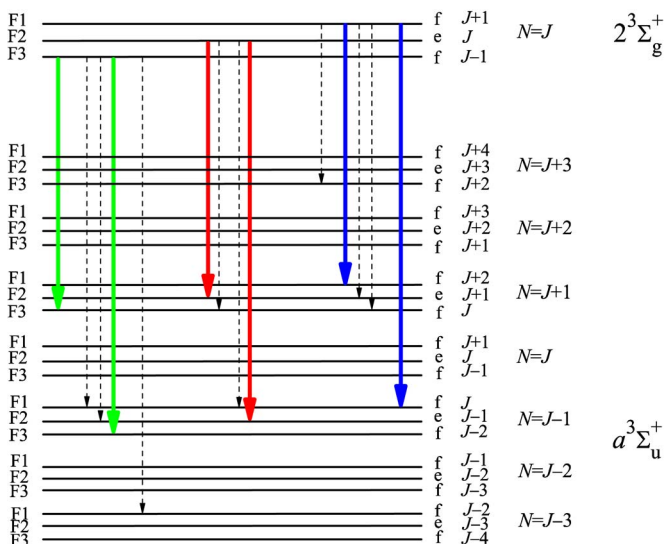


FIG. 4. Energy level diagram and relative intensities of $2^3\Sigma_g^+ \rightarrow a^3\Sigma_u^+$ transitions. The solid lines all have comparable intensities and the dashed lines have negligible intensities.

$J=71 \leftarrow b^3\Pi_{0u} v'=20$, $J'=70$ and $2^3\Sigma_g^+ v=40$, $N=71$, $J=71 \leftarrow b^3\Pi_{0u} v'=20$, $J'=70$ excitation lines are comparable, the intensity of the $2^3\Pi_{0g} v=16$, $J=71 \leftarrow b^3\Pi_{0u} v'=20$, $J'=72$ line is strong but the $2^3\Sigma_g^+ v=40$, $N=71$, $J=71 \leftarrow b^3\Pi_{0u} v'=20$, $J'=72$ line is much weaker in the excitation spectrum.

Figure 4 gives the energy level diagram and relative intensities of the $2^3\Sigma_g^+ \rightarrow a^3\Sigma_u^+$ bound-bound transitions.¹⁸ The solid lines all have comparable intensities while the dashed lines have negligible intensities. It can be seen that $2^3\Sigma_g^+ v$, $N, J \rightarrow a^3\Sigma_u^+ v'$ transitions from unperturbed upper levels [see e.g., Fig. 7(b)] result in two nearly equal intensity lines. This kind of doublet structure has also been observed in many resolved $2^3\Pi_g v, J \rightarrow a^3\Sigma_u^+ v'$ fluorescence spectra involving unperturbed $2^3\Pi_g v, J$ levels (see Refs. 5–7). In the resolved fluorescence spectra from $2^3\Sigma_g^+ \sim 2^3\Pi_g$ mixed levels [Fig. 2(c)], not only do the two lines have quite different intensities, but the relative intensities of the two lines are reversed for the two upper mixed levels even though the lower bound levels of the $a^3\Sigma_u^+$ state are not perturbed. In Fig. 2(c) we observe that for lower vibrational levels of the $a^3\Sigma_u^+$ state, each P line is stronger than the corresponding R line for the $2^3\Pi_{0g} v=16$, $J=71$ upper level, while each R line is stronger than the corresponding P line for the $2^3\Sigma_g^+ v=40$, $N=71$, $J=71$ upper level. However, this pattern reverses several times as the $a^3\Sigma_u^+$ state vibrational level increases. This anomaly has been observed in several resolved fluorescence spectra.

C. Fine and hyperfine structure

Hyperfine structure (HFS) of triplet Rydberg states of Li_2 , Na_2 , and NaK has been observed and analyzed.^{19–21} In the alkali diatomic molecules, the Fermi contact interaction is the dominant cause of the hyperfine splitting. In the homonuclear molecules, the Fermi contact constants of the Rydberg triplet states are all approximately equal to 1/4 of the Fermi contact constant of the atomic ground state.

The nuclear spin of the ^{39}K atom is 3/2, so the total nuclear spin of the $^{39}\text{K}_2$ molecule, I , is 3, 2, 1, or 0. For $I=3$ and 1, the nuclear spin wave functions are symmetric; they are antisymmetric for $I=2$ and 0. Since the total wave function has to be antisymmetric following the Pauli principle, the odd N levels of the $2^3\Sigma_g^+$ state of $^{39}\text{K}_2$ must combine with the symmetric nuclear wave functions with $I=3$ and 1 and the even N rotational levels must combine with the antisymmetric nuclear wave functions with $I=2$ and 0. The hyperfine structure of the $2^3\Sigma_g^+$ state is expected to follow the case $b_{\beta S}$ coupling scheme for low rotational levels. In this coupling scheme, the total nuclear spin I couples with total electron spin S to form $G(=S+I)$, and G couples with rotation N to form F . The odd N rotational levels should split into six hyperfine levels, $I=3, S=1, G=4, 3, 2$, and $I=1, S=1, G=2, 1, 0$, with energies $3b_F, -b_F, -4b_F$, and $b_F, -b_F, -2b_F$, respectively, according to the expression

$$E_{G,I,S} = \frac{b_F}{2} [G(G+1) - S(S+1) - I(I+1)],$$

where b_F is the Fermi contact constant. Thus the excitation spectra should exhibit five line patterns (since two levels are expected to be degenerate) for transitions involving antisymmetric (odd N) $2^3\Sigma_g^+$ rotational levels. Similarly, the symmetric (even N) rotational levels should split into four levels, $I=2, S=1, G=3, 2, 1$, and $I=0, S=1, G=1$, with energies $2b_F, -b_F, -3b_F$, and 0, respectively. Therefore, the even N levels should display four line patterns.

Figure 5 shows excitation spectra corresponding to several transitions into unperturbed $2^3\Sigma_g^+$ levels. The pattern is similar to that of the case $b_{\beta S}$ coupling of the Na_2 triplet states.^{20,22} The Fermi contact constant of the ^{39}K 4s ground state is much smaller than that of other alkali atoms:²³ ^7Li , 401.80 MHz; ^{23}Na , 885.7 MHz; ^{39}K , 231.54 MHz; ^{85}Rb , 1011.90 MHz; and ^{133}Cs , 2298.20 MHz. The HFS of several $\text{K}_2 b^3\Pi_{0u}$ levels has been resolved by laser excitation spectroscopy in a highly collimated molecular beam.²⁴ However, even though several K_2 triplet Rydberg states have been observed, no HFS has been previously resolved.^{5,6,25–27} In our sub-Doppler IR-IR double resonance excitation spectra of the $2^3\Sigma_g^+$ state, the HFS is partially resolved, as seen in Fig. 5.

With a simple calculation from the G splittings in Fig. 5, similar to that described in Ref. 28, we have obtained a primary Fermi contact constant, $b_F=65 \pm 10$ MHz. This is in good agreement with 1/4 of the atomic potassium ground state Fermi contact constant $[(1/4)231.54 \approx 58$ MHz]. Detailed analysis and simulations of the hyperfine structure will be published separately.

Perturbations involving levels of the $2^3\Pi_g$ state affect the fine-hyperfine splittings of the $\text{K}_2 2^3\Sigma_g^+$ levels similar to that observed for the $\text{Na}_2 3\Sigma_g^+$ states.²⁰ The hyperfine patterns of excitation lines into perturbed levels exhibit case $b_{\beta J}$ coupling. Figure 6 shows hyperfine patterns of perturbed $\text{K}_2 2^3\Sigma_g^+$ rotational lines displaying case $b_{\beta J}$ coupling. In all these cases, excitation lines associated with the F_2 component are narrower than the lines involving the F_1 and F_3 fine structure components. The energies of the F_1 and F_3 components can be either higher or lower than that of the F_2 com-

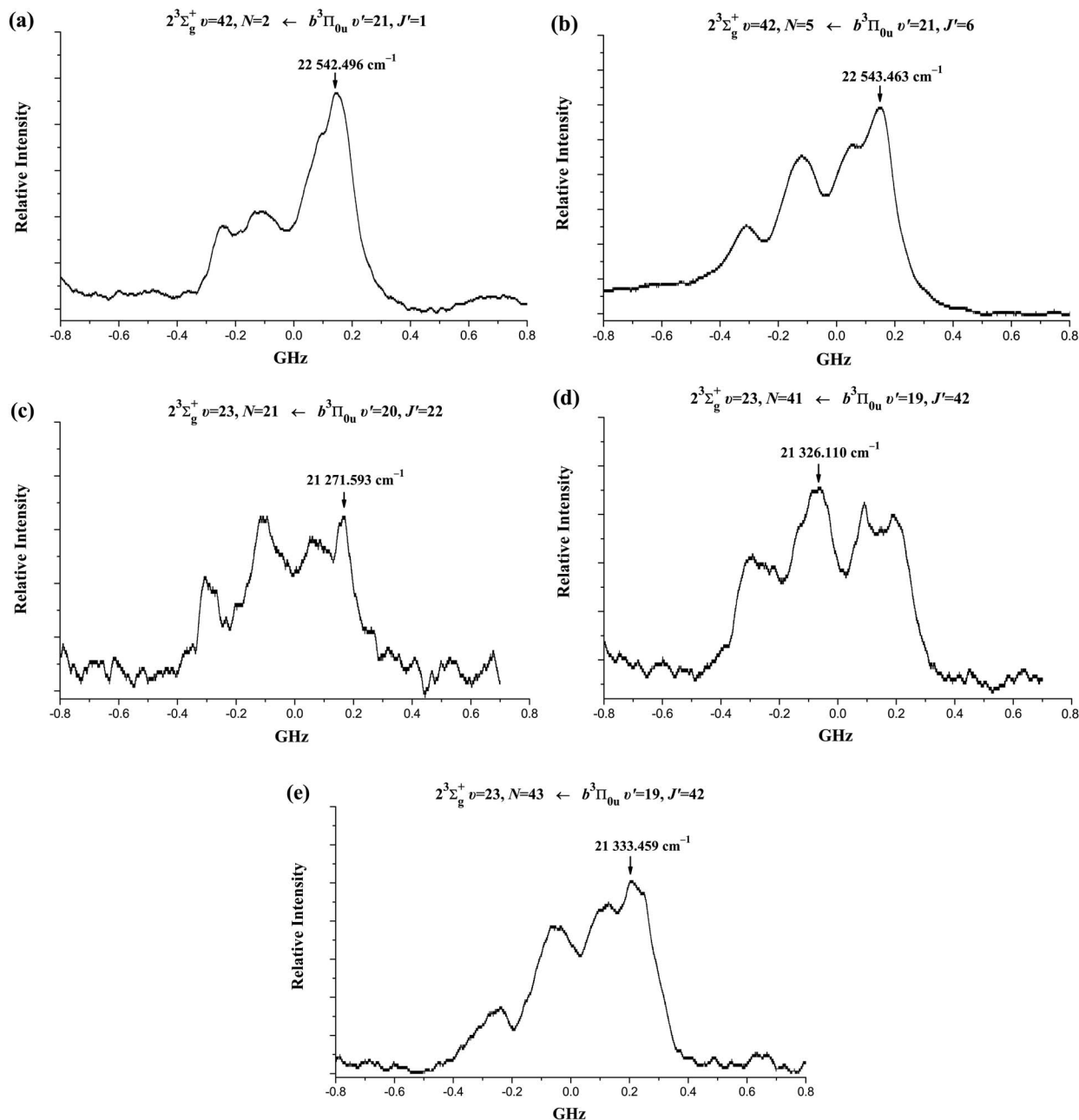


FIG. 5. Excitation line shapes of transitions: (a) $2^3\Sigma_g^+ v=42, N=2 \leftarrow b^3\Pi_{0u} v'=21, J'=1$; (b) $2^3\Sigma_g^+ v=42, N=5 \leftarrow b^3\Pi_{0u} v'=21, J'=6$; (c) $2^3\Sigma_g^+ v=23, N=21 \leftarrow b^3\Pi_{0u} v'=20, J'=22$; (d) $2^3\Sigma_g^+ v=23, N=41 \leftarrow b^3\Pi_{0u} v'=19, J'=42$; and (e) $2^3\Sigma_g^+ v=23, N=43 \leftarrow b^3\Pi_{0u} v'=19, J'=42$. Labeled arrows give the term energies of the indicated peaks.

ponent due to these perturbations of the $2^3\Sigma_g^+$ levels by nearby $2^3\Pi_g$ levels of the same J . Since the $2^3\Sigma_g^+ \sim 2^3\Pi_g$ perturbation comes from L uncoupling $[(1/2\mu R^2)(\mathbf{J}^+\mathbf{L}^- + \mathbf{J}^-\mathbf{L}^+)]$,¹⁷ all higher $2^3\Sigma_g^+$ rotational levels above the $2^3\Pi_g v=0$ level observed in our experiment have case b_{BJ} coupling (Fig. 6), while $2^3\Sigma_g^+$ rotational levels (up to at least $N=43$) which lie below the potential minimum of the $2^3\Pi_g$ state and other relatively unperturbed $2^3\Sigma_g^+$ levels all have case b_{BS} coupling (Fig. 5).

In addition to perturbations involving the $2^3\Pi_g$ state, the spin-rotation interaction, which is not important for low- N $2^3\Sigma_g^+$ rotational levels, becomes inevitably stronger with increasing rotational quantum number and the coupling scheme is expected to evolve from case b_{BS} toward case b_{BJ}

as N increases. This transition from case b_{BS} to case b_{BJ} has not been observed in the unperturbed rotational levels up to $N=43$. For the perturbed levels, the observed splitting of a particular $2^3\Sigma_g^+$ level also depends on how strongly it interacts with a perturbing $2^3\Pi_g$ level. In Fig. 6(c) the $2^3\Sigma_g^+ v=42, N=63, J=63$ level is perturbed by the $2^3\Pi_{1g} v=18, J=63$ level, which lies 2.349 cm^{-1} below the $2^3\Sigma_g^+ v=42, N=63, J=63$ level.

D. Two-photon transition assignment

Many two-photon transitions into the $2^3\Pi_g$ state have been observed and some of them have been assigned.^{5,6} We observed a two-photon transition at $11\,539.361 \text{ cm}^{-1}$.²⁹ Fig-

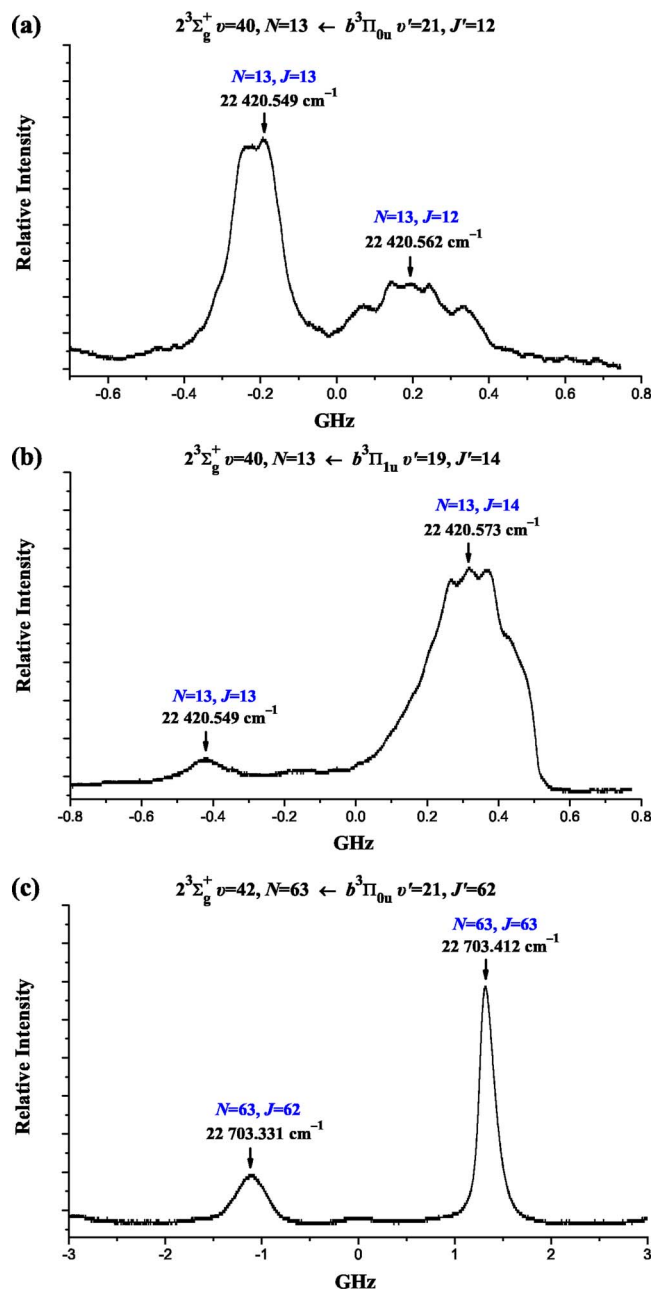


FIG. 6. Excitation line shapes of the following transitions: (a) $2^3\Sigma_g^+ v=40, N=13 \leftarrow b^3\Pi_{0u} v'=21, J'=12$; (b) $2^3\Sigma_g^+ v=40, N=13 \leftarrow b^3\Pi_{1u} v'=19, J'=14$; and (c) $2^3\Sigma_g^+ v=42, N=63 \leftarrow b^3\Pi_{0u} v'=21, J'=62$. Labeled arrows give the term energies of the indicated peaks.

ure 7(a) shows the resolved fluorescence spectrum from the upper level excited by two $11\,539.361\text{ cm}^{-1}$ photons, which again displays the double oscillation pattern. In order to confirm that the oscillating continuum at $\lambda > 580\text{ nm}$ is indeed also due to a K_2 two-photon transition, we also recorded resolved fluorescence using the same laser frequency to excite molecules in a mixed sodium-potassium heat pipe. The relative intensity of the longer wavelength oscillating band compared to the known K_2 $2^3\Pi_g \rightarrow a^3\Sigma_u^+$ band in the $545\text{--}575\text{ nm}$ region was the same in the two heat pipes. This indicates that the source of the longer wavelength band is indeed K_2 rather than NaK , which is likely to be present in low concentration in the potassium heat pipe due to Na impurities.

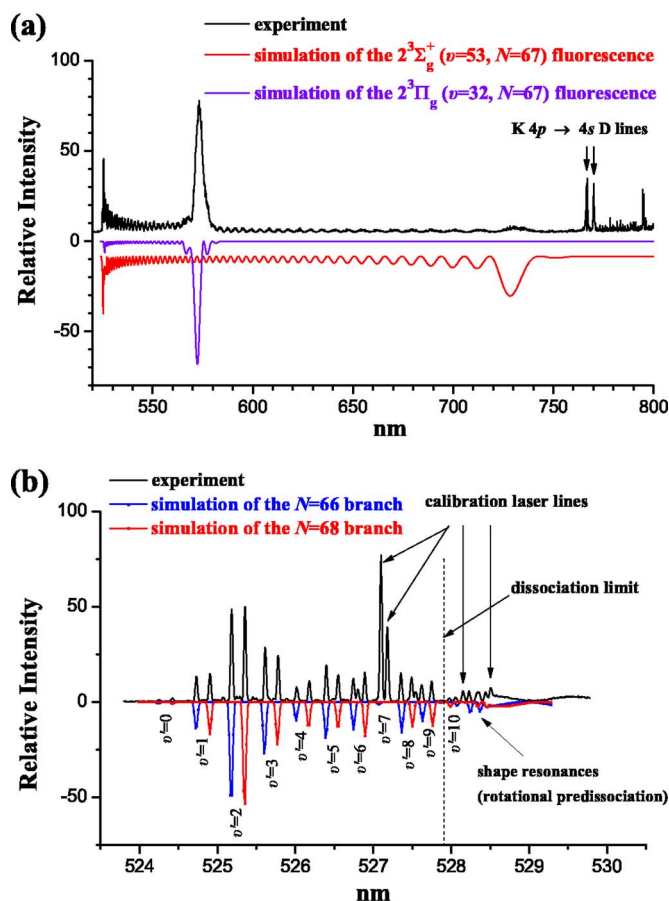


FIG. 7. (a) Resolved fluorescence spectrum from the excited triplet level ($^{39}\text{K}_2$ $2^3\Sigma_g^+ v=53, N=67$) populated by a two-photon transition at $11\,539.361\text{ cm}^{-1}$ and its simulation. The experimental intensities have not been corrected for the relative detection system efficiency vs wavelength. (b) Expanded portion of (a) showing transitions into the bound levels of the $a^3\Sigma_u^+$ state. This spectrum has been corrected for the relative detection system efficiency vs wavelength.

This two-photon transition spectrum looks very similar to the $2^3\Sigma_g^+ \rightarrow a^3\Sigma_u^+$ fluorescence of Figs. 2(a) and 3(b). The spectrum contains transitions into the bound levels of the $a^3\Sigma_u^+$ state as well as a diffuse band associated with the $a^3\Sigma_u^+$ state repulsive continuum. The fluorescence into the vibrational levels of the $a^3\Sigma_u^+$ state [Fig. 7(b)] consists of a series of doublets. The discrete lines in Fig. 7(b) have been assigned to transitions into vibrational levels of the $a^3\Sigma_u^+$ state, including ($v > 10$) rotationally predissociated shape resonance states.

Using the procedure of Ref. 5, we have determined that the two-photon transition at $11\,539.361\text{ cm}^{-1}$ is the $^{39}\text{K}_2$ $2^3\Sigma_g^+ v=53, N=67 \leftarrow b^3\Pi_{0u} v'=19, J'=68 \leftarrow X^1\Sigma_g^+ v''=0, J''=69$ transition.

In our attempt to excite this $2^3\Sigma_g^+ v=53, N=67$ level via the $b^3\Pi_{0u} v'=29, 30, J'=68/66$ intermediate levels (excited from the $X^1\Sigma_g^+ v''=7/8, J''=67/69$ ground state levels) no signal was detected at the predicted energy, probably due to small Franck-Condon factors and relatively small populations in the $X^1\Sigma_g^+ v''=7/8, J''=67/69$ levels. Therefore, in order to confirm the above assignment, we set the pump laser frequency to $11\,539.361\text{ cm}^{-1}$ and used the probe laser to depopulate the intermediate level by exciting the $2^3\Pi_{0g} v$

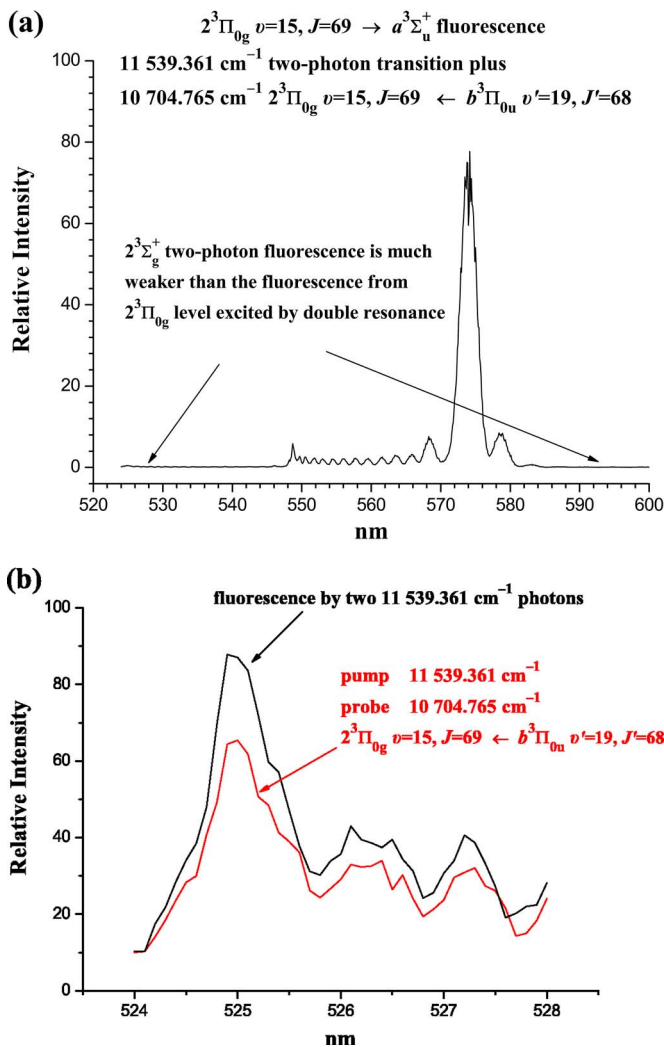


FIG. 8. (a) Resolved fluorescence to the $a^3\Sigma_u^+$ state with the pump laser frequency set to $11\,539.361\text{ cm}^{-1}$ while the probe laser excited the $2^3\Pi_{0g} v=15, J=69 \leftarrow b^3\Pi_{0u} v'=19, J'=68$ transition ($10\,704.765\text{ cm}^{-1}$); (b) $524\text{--}528\text{ nm}$ fluorescence with and without the $10\,704.765\text{ cm}^{-1}$ probe laser when the pump laser was set to $11\,539.361\text{ cm}^{-1}$

$=15, J=69 \leftarrow b^3\Pi_{0u} v'=19, J'=68$ transition. Figure 8(a) shows the fluorescence detected with both lasers. The $2^3\Pi_{0g} v=15, J=69 \rightarrow a^3\Sigma_u^+$ fluorescence is much stronger than the two-photon fluorescence induced by the pump laser with our diode laser power (40 mW). Figure 8(b) shows the fluorescence in the wavelength region of $524\text{--}528\text{ nm}$ [bound-bound lines, see Fig. 7(b)] detected with and without the probe laser. It is clear that when the probe laser excited the $2^3\Pi_{0g} v=15, J=67/69 \leftarrow b^3\Pi_{0u} v'=19, J'=68$ transitions, the $524\text{--}528\text{ nm}$ fluorescence decreased by about 20%. [Note that the $2^3\Pi_{0g} v=15, J=67/69$ levels do not radiate in the $524\text{--}528\text{ nm}$ region.] Considering the probe laser power was only 20 mW and the two lasers were not very well overlapped (the diode lasers have dumbbell-like spatial mode patterns), this 20% decrease clearly indicates that the molecule responsible for the two-photon induced fluorescence is $^{39}\text{K}_2$, the intermediate enhancing level is the $b^3\Pi_{0u} v'=19, J'=68$ level, and the upper level has an energy of $23\,393.781\text{ cm}^{-1}$. Energy levels of the nearby $2^3\Pi_g v=32$ levels have been observed. Thus this upper level excited by

TABLE I. Molecular constants of the $\text{K}_2\ 2^3\Sigma_g^+$ state. All quantities are in cm^{-1} except R_e , which is in \AA . Semiclassical estimate (Ref. 17) $Y_{02} \approx -4Y_{01}^3/Y_{10}^2 = -6.563 \times 10^{-8}\text{ cm}^{-1}$. The numbers of digits presented are necessary for an accurate reproduction of the term values obtained in the fit and do not reflect the uncertainty in the individual molecular constants.

	This work	<i>ab initio</i> (Ref. 8)
$T_e + Y_{00}$	19 471.088 9	19 376
Y_{10}	79.714 824	78.55
Y_{20}	-0.159 034 8	
Y_{30}	$-3.837\,76 \times 10^{-4}$	
Y_{01}	0.047 064 95	0.047 72
Y_{11}	$-1.596\,70 \times 10^{-4}$	
Y_{21}	$4.378\,1 \times 10^{-7}$	
Y_{31}	$-1.091\,1 \times 10^{-8}$	
Y_{02}	-6.952×10^{-8}	
R_e	4.288	4.258
Y_{00}	0.005 3	

two $11\,539.361\text{ cm}^{-1}$ photons must be the $^{39}\text{K}_2\ 2^3\Sigma_g^+ v, N \sim 67$ or 69 level. We also set the probe laser frequencies to excite the $b^3\Pi_{0u} v'=19, J'=68 \leftarrow X^1\Sigma_g^+ v''=9, J''=67$ and $b^3\Pi_{0u} v'=19, J'=68 \leftarrow X^1\Sigma_g^+ v''=11, J''=67$ transitions to see if the fluorescence of $524\text{--}528\text{ nm}$ in Fig. 8(b) increased. But we did not detect a clear increase, most probably due to the small thermal population of the $X^1\Sigma_g^+ v''=9/11, J''=67$ levels under our experimental conditions.

The bound-bound fluorescence shown in Fig. 7(b) has been carefully corrected for the relative detection system efficiency versus wavelength. The $a^3\Sigma_u^+$ state potential energy function has been reported in Ref. 28, and we have used this to predict rovibrational term values. From the P - R fluorescence line separation, the upper level has been determined to have rotational quantum number $N=67$. The fluorescence frequencies into the $a^3\Sigma_u^+$ bound levels also confirm the energy of the upper $2^3\Sigma_g^+$ level.

While the highest vibrational level of the $2^3\Sigma_g^+$ state observed by IR-IR double resonance is $v=47$, this two-photon excited level $v=53, N=67$ is the highest detected level of the $2^3\Sigma_g^+$ state.

E. Molecular constants and RKR potential curve

In total, we have observed 845 transitions into the $^{39}\text{K}_2\ 2^3\Sigma_g^+ v=23\text{--}25, 27, 28, 31\text{--}33, 38\text{--}45, 47,$ and 53 levels. The PFOODR excitation data are provided in a supplementary table, which has been placed in the Electronic Physics Auxiliary Publication Service (EPAPS).³⁰ A direct Dunham fit of the experimental term values produced a preliminary set of molecular constants and the corresponding Rydberg-Klein-Rees (RKR) potential function. However, a simulation of the experimentally observed bound-free continua of $2^3\Sigma_g^+ \rightarrow a^3\Sigma_u^+$ transitions using this $2^3\Sigma_g^+$ RKR function and the $a^3\Sigma_u^+$ potential function from Ref. 28 showed that the node positions in the calculated and observed spectra differed significantly in the long-wavelength region. An attempt to improve the situation by a correction of the short-range branch of the $a^3\Sigma_u^+$ potential alone was unsuccessful. Therefore, we used an expanded version of the global fit procedure of Ref. 28, in which the experimental term values of the

TABLE II. The RKR potential curve of the K_2 $2^3\Sigma_g^+$ state derived from the constants of Table I. $R_e=4.288$ Å, $T_e=19471.083$ 6 cm^{-1} , $v_{\min}=-0.500$ 07, $Y_{00}=0.005$ 3 cm^{-1} .

R_{\min} (Å)	R_{\max} (Å)	T_e+G_v (cm^{-1})	v
4.145 28	4.440 23	19 510.906 5	0
4.046 83	4.558 53	19 590.302 0	1
3.981 76	4.643 48	19 669.376 0	2
3.930 43	4.714 73	19 748.126 2	3
3.887 13	4.777 99	19 826.550 2	4
3.849 26	4.835 86	19 904.645 8	5
3.815 36	4.889 80	19 982.410 7	6
3.784 54	4.940 72	20 059.842 5	7
3.756 17	4.989 24	20 136.939 0	8
3.729 83	5.035 78	20 213.697 8	9
3.705 20	5.080 69	20 290.116 7	10
3.682 03	5.124 19	20 366.193 4	11
3.660 12	5.166 50	20 441.925 5	12
3.639 34	5.207 77	20 517.310 7	13
3.619 54	5.248 13	20 592.346 8	14
3.600 62	5.287 69	20 667.031 4	15
3.582 51	5.326 54	20 741.362 3	16
3.565 12	5.364 75	20 815.337 1	17
3.548 39	5.402 41	20 888.953 6	18
3.532 27	5.439 55	20 962.209 4	19
3.516 70	5.476 25	21 035.102 2	20
3.501 66	5.512 54	21 107.629 7	21
3.487 09	5.548 46	21 179.789 6	22
3.472 98	5.584 06	21 251.579 7	23
3.459 28	5.619 36	21 322.997 6	24
3.445 98	5.654 40	21 394.041 0	25
3.433 05	5.689 20	21 464.707 6	26
3.420 47	5.723 79	21 534.995 2	27
3.408 22	5.758 20	21 604.901 3	28
3.396 28	5.792 45	21 674.423 8	29
3.384 65	5.826 55	21 743.560 2	30
3.373 30	5.860 53	21 812.308 4	31
3.362 22	5.894 41	21 880.665 9	32
3.351 41	5.928 20	21 948.630 5	33
3.340 84	5.961 92	22 016.200 0	34
3.330 51	5.995 58	22 083.371 9	35
3.320 42	6.029 21	22 150.144 0	36
3.310 55	6.062 81	22 216.514 0	37
3.300 89	6.096 40	22 282.479 5	38
3.291 44	6.129 99	22 348.038 4	39
3.282 20	6.163 59	22 413.188 2	40
3.273 15	6.197 23	22 477.926 7	41
3.264 29	6.230 90	22 542.251 5	42
3.255 61	6.264 62	22 606.160 5	43
3.247 12	6.298 41	22 669.651 2	44
3.238 80	6.332 27	22 732.721 3	45
3.230 66	6.366 22	22 795.368 7	46
3.222 68	6.400 27	22 857.590 8	47
3.214 87	6.434 42	22 919.385 6	48
3.207 22	6.468 69	22 980.750 5	49
3.199 73	6.503 09	23 041.683 5	50
3.192 40	6.537 63	23 102.182 0	51
3.185 22	6.572 32	23 162.244 0	52
3.178 20	6.607 18	23 221.866 9	53
3.171 32	6.642 20	23 281.048 6	54
3.164 60	6.677 41	23 339.786 8	55

$2^3\Sigma_g^+$ state and the node positions of the spectra from Figs. 1 and 7 were included into the set of the experimental data, and the potential functions of the $2^3\Sigma_g^+$, $a^3\Sigma_u^+$, $3^3\Pi_g$, and $4^3\Sigma_g^+$ states were corrected to give the best fit. The details of this fit along with new data for states other than $2^3\Sigma_g^+$ will be published separately.³¹

Molecular constants of the $2^3\Sigma_g^+$ state are given in Table I. Table II gives the experimental $2^3\Sigma_g^+$ RKR potential curve determined from the global fitting procedure in this work. Figures 1 (spectrum D), 7(a) and 7(b) show final simulated resolved fluorescence spectra in comparison with observed spectra. From the direct Dunham fit we found the uncertainty of the T_e value to be 0.7 cm^{-1} , since the lowest vibrational level observed is $v=23$. However, in Table I we list more digits for the constants than are needed to reflect the accuracy with which any particular constant has been determined, since these extra digits are needed to reproduce the observed term values and bound-free node positions to within experimental uncertainties.

IV. CONCLUSION

Ab initio calculations⁸ indicate that the K_2 $2^3\Sigma_g^+$ state dissociates to the $4s+5s$ atomic limit and predict values $R_e=4.258$ Å and $T_e=19376$ cm^{-1} above the potential minimum of the ground state. Limited by the available laser wavelengths, the $v=23-25$, 27, 28, 31-33, 38-45, 47, and 53 levels have been observed by perturbation-facilitated IR-IR double resonance spectroscopy and two-photon excitation. Vibrational numbering has been determined from resolved fluorescence spectra into the $a^3\Sigma_u^+$ state. Molecular constants have been obtained using a global fit procedure based on a comprehensive set of experimental data, which includes node positions of the bound-free continua as well as term values.

Fine and hyperfine splittings have been resolved in the excitation spectra. The $2^3\Sigma_g^+$ state follows case $b_{\beta S}$ coupling for unperturbed levels up to $N=43$. Fermi contact is the dominant hyperfine interaction and a preliminary Fermi contact constant, $b_F=65\pm 10$ MHz, has been obtained.

Perturbations between the $2^3\Sigma_g^+$ and $2^3\Pi_g$ states were observed. The hyperfine patterns of the $2^3\Sigma_g^+$ levels are strongly affected by perturbation. Intensity anomalies of rotational lines due to quantum-mechanical interference effects appeared both in the $2^3\Sigma_g^+\sim 2^3\Pi_g\leftarrow b^3\Pi_u$ excitation spectra and in the $2^3\Sigma_g^+\sim 2^3\Pi_g\rightarrow a^3\Sigma_u^+$ resolved fluorescence spectra.

ACKNOWLEDGMENTS

Support from the NSFC (20473042) and SRFDP of China, the RFBR (05-03-39012) of Russia, and NSF (USA) is gratefully acknowledged. The authors thank Dr. Patrick Burns for assistance with the mixed sodium-potassium heat pipe experiment.

¹L. Li and R. W. Field, J. Phys. Chem. **87**, 3020 (1983).

²L. Li and R. W. Field, in *Molecular Spectroscopy and Dynamics by Stimulated Emission Pumping*, edited by H. L. Dai and R. W. Field (World Scientific, Singapore, 1995), Chap. 7.

³L. Li and A. M. Lyyra, Spectrochim. Acta, Part A **55**, 2147 (1999), and references therein.

⁴J. Huennekens, I. Prodan, A. Marks, L. Sibbach, E. Galle, T. Morgus, and L. Li, J. Chem. Phys. **113**, 7384 (2000), and the references therein.

⁵Y. Chu, F. Xie, D. Li, L. Li, V. B. Sovkov, V. S. Ivanov, and A. M. Lyyra, J. Chem. Phys. **122**, 074302 (2005).

⁶F. Xie, D. Li, Y. Chu, L. Li, V. B. Sovkov, V. S. Ivanov, and S. Magnier, J. Phys. Chem. A **110**, 11260 (2006).

⁷L. Li, P. Qi, A. Lazoudis, E. Ahmed, and A. M. Lyyra, Chem. Phys. Lett.

- 403**, 262 (2005).
- ⁸ S. Magnier, M. Aubert-Frecon, and A. R. Allouche, *J. Chem. Phys.* **121**, 1771 (2004).
- ⁹ X. Xie and R. W. Field, *J. Mol. Spectrosc.* **117**, 228 (1986).
- ¹⁰ L. Li and R. W. Field, *J. Mol. Spectrosc.* **117**, 245 (1986).
- ¹¹ G. Pichler, J. T. Bahns, K. Sando, W. C. Stwalley, D. D. Konowalow, L. Li, R. W. Field, and W. Muller, *Chem. Phys. Lett.* **129**, 425 (1986).
- ¹² R. S. Mulliken, *J. Chem. Phys.* **55**, 309 (1971).
- ¹³ J. Tellinghuisen, G. Pichler, W. L. Snow, M. E. Hillard, and R. J. Exton, *Chem. Phys.* **50**, 313 (1980).
- ¹⁴ J. T. Bahns, W. C. Stwalley, and G. Pichler, *J. Chem. Phys.* **90**, 2841 (1989).
- ¹⁵ W.-T. Luh, J. T. Bahns, A. M. Lyyra, K. M. Sando, P. D. Kleiber, and W. C. Stwalley, *J. Chem. Phys.* **88**, 2235 (1988), and the references therein.
- ¹⁶ C. Radzewicz, P. Kowalczyk, and J. Krasinski, *Z. Phys. A* **314**, 293 (1983).
- ¹⁷ H. Lefebvre-Brion and R. W. Field, *The Spectra and Dynamics of Diatomic Molecules* (Elsevier, New York, 2004).
- ¹⁸ I. Kovács, *Rotational Structure in the Spectra of Diatomic Molecules* (Hilger, London, 1969).
- ¹⁹ L. Li, A. Lazoudis, P. Yi, Y. Liu, J. Huennekens, R. W. Field, and A. M. Lyyra, *J. Chem. Phys.* **116**, 10704 (2002), and references therein.
- ²⁰ Y. Liu, L. Li, G. Lazarov, A. Lazoudis, A. M. Lyyra, and R. W. Field, *J. Chem. Phys.* **121**, 5821 (2004).
- ²¹ P. Burns, A. D. Wilkins, A. P. Hickman, and J. Huennekens, *J. Chem. Phys.* **122**, 074306 (2005).
- ²² G. Lazarov, A. M. Lyyra, L. Li, and J. Huennekens, *J. Mol. Spectrosc.* **196**, 259 (1999).
- ²³ L. Tterlikkis, S. D. Mahanti, and T. P. Das, *Phys. Rev.* **176**, 10 (1968).
- ²⁴ C. Lisdat, H. Knockel, and E. Tiemann, *J. Mol. Spectrosc.* **199**, 81 (2000).
- ²⁵ L. Li, A. M. Lyyra, W. T. Luh, and W. C. Stwalley, *J. Chem. Phys.* **93**, 8452 (1990).
- ²⁶ J. Kim, H. Wang, C. Tsai, J. Bahns, W. Stwalley, G. Jong, and A. M. Lyyra, *J. Chem. Phys.* **102**, 6646 (1995).
- ²⁷ J. Magnes, E. Ahmed, T. Kirova, C. Goldberg, A. M. Lyyra, S. Magnier, Y. Liu, and L. Li, *J. Mol. Spectrosc.* **221**, 72 (2003).
- ²⁸ E. Ahmed, A. M. Lyyra, F. Xie, D. Li, Y. Chu, L. Li, V. S. Ivanov, V. B. Sovkov, and S. Magnier, *J. Mol. Spectrosc.* **234**, 41 (2005).
- ²⁹ The $11\,539.361\text{ cm}^{-1}$ two-photon transition was first observed with Ti:sapphire laser (Coherent model 899-29) excitation with the laser frequency calibrated using a uranium hollow cathode lamp. In the experiment with diode lasers, the laser frequencies were measured using Burleigh WA-1600 wavemeters, which have a specified accuracy of 0.003 cm^{-1} . The two-photon transition frequency was measured by a WA-1600 wavemeter to be $11\,539.365\text{ cm}^{-1}$. $11\,539.365\text{ cm}^{-1}$ is also the central frequency of the $b^3\Pi_{0u}v'=19, J'=68 \leftarrow X^1\Sigma_g^+v''=0, J''=69$ transition according to Refs. 32–34.
- ³⁰ See EPAPS Document No. E-JCPSA6-126-027717 for the PFOODR excitation data. This document can be reached via a direct link in the online article's HTML reference section or via the EPAPS homepage (<http://www.aip.org/pubservs/epaps.html>).
- ³¹ V. B. Sovkov, V. S. Ivanov, D. Li, F. Xie, L. Li, *Opt. Spectrosc.* (to be published).
- ³² C. Amiot, J. Verges, and C. E. Fellows, *J. Chem. Phys.* **103**, 3350 (1995).
- ³³ M. R. Manaa, A. J. Ross, F. Martin, P. Crozet, A. M. Lyyra, L. Li, C. Amiot, and T. Bergeman, *J. Chem. Phys.* **117**, 11208 (2002).
- ³⁴ C. Amiot, *J. Mol. Spectrosc.* **147**, 370 (1991).